The Lanthanum–Germanium System. Nineteen Isostructural Interstitial Compounds of the La_5Ge_3 Host

Arnold M. Guloy and John D. Corbett*

Ames Laboratory-DOE[1] and Department of Chemistry, Iowa State University, Ames, Iowa 50011

Received December 29, 1992

Sintering reactions in sealed Ta containers afford single-phase interstitial derivatives La_5Ge_3Z of the line compound La_5Ge_3 (Mn_5Si_3 type) for Z = B_x, C_x, N, O, P, S, Cl, As, Se, Sb, Cr, Mn, Fe, Co, Ni, Cu, Zn, Ru, and Cd. Guinier X-ray techniques were not sufficiently sensitive to discern the exact stoichiometries of the boron and carbon examples, but x probably falls in the ranges 0.7 ± 0.1 and 0.7–1.0, respectively. The lattice dimensions and relative inertness previously reported for some La_5Ge_3 samples appear to be those of La_5Ge_3O, including for the germaniothermal synthesis from La_2O_3 and Ge. Single crystal X-ray studies were carried out for La_5Ge_3 and La_5Ge_3Cr ($P6_3/mcm$, $Z = 2$, a = 8.941 (1), 9.004 (1) Å, c = 6.878 (1), 7.105 (1) Å, R/R_w = 3.4/3.8, 2.4/2.9%, respectively). The short La–Cr distance in the latter, 2.801 (1) Å, is distinctive. Cell volumes increase on Z insertion into La_5Ge_3 for all but N and O. The changes within the Zn–Se series of Z are markedly greater than in electron-richer zirconium host analogues. La_5Ge_3 is Pauli-paramagnetic and metallic, while La_5Ge_3P is a diamagnetic semiconductor (Zintl phase) appropriate to the presence of just three excess (conduction) electrons in the La_5Ge_3 host. Extended-Hückel band calculation results for La_5Ge_3 and La_5Ge_3P are consistent with these properties. Valence and conduction band overlap that is present in La_5Ge_3 through strong La–Ge bonding and large band dispersions is removed on oxidation with P. Calculations for the more electropositive Fe interstitial place the unsplit Fe d levels near E_F, with Fe 4s providing much of the binding. La_3Ge has a Ti_3P-type structure.

Introduction

Among the numerous intermetallic compounds known, those formed between the early transition (or pretransition) metals and the post-transition metals (or neighboring metalloids) exhibit several characteristics that aid the chemist in categorizing their expected electronic properties and chemical bonding. Much of this facility derives from the polar nature of these compounds which comes from the appreciable differences in electronegativities and valence energies of the two types of elements. The closed-shell electronic limit in these phases is achieved when there is a balance between the number of valence electrons available from the electropositive component and those required by the lower lying valence states of the post-transition components, which may be present as separate atoms or form some sort of interconnected polyanionic network. This kind of valence compound is frequently designated a Zintl phase after the early concepts of Zintl[2,3] as expanded by Klemm.[4,5] The variety of compositions and structures that follow these simple concepts is remarkable indeed.[6] Of course, the underlying strong covalent bonding between the two (or more) atom types in such polar compounds is general and not pertinent just at the Zintl limit. Thus many similar compounds with an excess of electrons may still be usefully described as "metallic Zintl phases".[7]

An attractive structure type in which chemical versatilities allow the exploration of a particularly wide range of electronic counts and factors is known as the Mn_5Si_3 type, for which ~170 A_5M_3 examples are reported for metal A from groups 2–6 and M principally from the main-group aluminum, silicon, and arsenic families.[8] The most pertinent feature of this structure is the quasi-infinite but interbridged A_3M_3 chains composed of confacial $A_{6/2}$ antiprisms on which separate M atoms bridge the edges of the shared faces. In this case, excess electrons remaining after the valence states on M are filled are reasonably assumed to occupy conduction band states based primarily on A.[9] The condensed cluster unit is much like that in the Chevrel chain phases,[10] but with one important distinction: a variety of heteroatoms may also be bound in the centers of the antiprisms in many, if not all, Mn_5Si_3-type examples without any change in lattice type. These "stuffed" ternary examples were originally described as Novotny phases based on the idea that the interstitial Z in $A_5M_3Z_x$ was essential for stability; a variable x was also thought possible, especially with the lighter Z, and therefore $A_5M_3Z_x$ homogeneity ranges.[11,12]

Subsequent investigations with more modern reagents, equipment, and capabilities have shown that these last premises are not often correct. Many examples of true binaries exist in this structure type with only a few exceptions, La_5Sn_3O for example,[13] and numerous "stuffed" A_5M_3Z derivatives appear to have substantially fixed compositions. We have earlier learned how to quantitatively synthesize the pure refractory phases in the series Zr_5Sb_3Z,[14] Zr_5Sn_3Z,[15] and Zr_5Pb_3Z[16] in which Z in each case may range over 15–20 main-group and late transition-metal elements. These are all electron rich and metallic, and as such offer interesting opportunities to systematically vary the properties of a family of metallic compounds in a single structure type. Use of earlier transition metals as the A component affords host phases with fewer surplus electrons and the attractive possibility that

(1) This research was supported by the Office of the Basic Energy Sciences, Materials Sciences Division, U.S. Department of Energy. The Ames Laboratory is operated for DOE by Iowa State University under Contract No. W-7405-Eng-82.

(2) Zintl, E. *Angew. Chem.* **1939**, *52*, 1.
(3) Laves, F. *Naturwissenschaften* **1941**, *29*, 244.
(4) Klemm, W. *Proc. Chem. Soc. London* **1958**, 329.
(5) Klemm, W.; Busmann, E. *Z. Anorg. Allg. Chem.* **1963**, *319*, 297.
(6) Schäfer, H. *Annu. Rev. Mater. Sci.* **1985**, *15*, 1.
(7) Nesper, R. *Angew. Chem., Int. Ed. Eng.* **1991**, *30*, 789.
(8) Villars, P.; Calvert, L. D. *Pearson's Handbook of Crystallographic Data for Intermetallic Phases*, 2nd ed.; American Society for Metals International: Metals Park, OH, 1991; pp 230, 255, 1789, 4212.
(9) Garcia, E.; Corbett, J. D. *Inorg. Chem.* **1988**, *27*, 2353.
(10) Potel, M.; Chevrel, R.; Sergent, M.; Armici, J. C.; Decroux, M.; Fischer, Ø, *J. Solid State Chem.* **1980**, *53*, 286.
(11) Novotny, H.; Benesovsky, F. In *Phase Stability in Metals and Alloys*; Rudman, P. S.; Stringer, J.; Jaffee, R. I., Eds.; McGraw-Hill: New York, 1966; pp 319–336.
(12) Parthé, E. *Powder Metall. Bull.* **1957**, *8*, 23, 33.
(13) Kwon, Y.-U.; Rzeznik, M.; Guloy, A.; Corbett, J. D. *Chem. Mater.* **1990**, *2*, 546.
(14) Garcia, E.; Corbett, J. D. *Inorg. Chem.* **1990**, *29*, 3274.
(15) Kwon, Y.-U.; Corbett, J. D. *Chem. Mat.* **1992**, *4*, 1348.
(16) Kwon, Y.-U.; Corbett, J. D. *J. Alloys Comp.* **1993**, *190*, 219.

0020-1669/93/1332-3532$04.00/0

suitable Z interstitials may be used to "tune" the electron counts of metallic hosts down to zero, thereby yielding semiconducting Zintl phases. This approach has already been explored in a limited way for compounds of the alkaline-earth metals Ca, Sr, and Ba in combination with Sb or Bi. In these cases, Zintl phases are obtained in a stuffed Mn_5Si_3 (=Ti_5Ga_4[8]) structure type for Cl and Br and in other structures for F, I, and H.[17,18]

The present article reports studies with similar objectives for the host La_5Ge_3 where a much greater versatility regarding Z may be obtained. The three electrons per formula unit that nominally remain after the Ge-based valence bands are filled ($5 \times 3 - 3 \times 4$) allow a more extensive probing of the host's conduction band with a variety of Z elements. Thus more electronegative elements may be used to "soak up" some or all of these electrons and localize them in low-lying La–Z states with primarily Z character. On the other hand, valence states of more metallic Z elements presumably lie closer to E_F. We chose lanthanum for the first element in order to have a diamagnetic host against which Pauli-like susceptibilities could be discerned and germanium for the second largely because its compounds had been explored much less than the corresponding silicides. The progress of carbon reactions with some of these rare-earth metal (R) silicides[19-22] and germanides[23] have been examined before, but no quantitative data on structures, compositions, or properties have been reported.

A brief examination of the entire La–Ge system was also undertaken since purities of the somewhat air-sensitive lanthanum and the synthetic conditions in general have not always been carefully controlled or considered in previous work.[24,25] In fact, contradictions among the lattice constants and properties reported for La_5Ge_3[26-31] are often symptomatic of impurities in this particular type of structure. There have also been interesting, even surprising, claims that La_5Ge_3, $LaGe_2$, and other R_5Ge_3 phases can be obtained directly from germaniothermal reactions of R_2O_3 with Ge, gaseous GeO being the other product.[30-32] Reports on our other studies of the La_5Tt_4 (Tt = tetregen) phases with Tt dimers as well as the analogous La_5Pb_3Z and the related $La_{15}Ge_9Z$ systems will be forthcoming.[33]

Experimental Section

Because of the sensitivity of the reagent La and of some of the products to oxygen and moisture, all reactants and products were handled and stored only in a N_2- or He-filled glove box or sealed in ampoules. The moisture in the box was regularly <1 ppm vol and, although the oxygen was not measured, exposed 60-watt light bulb filaments would burn therein for 12 h or more.

Materials. The lanthanum rod used was an Ames Laboratory product (five 9's) with principal impurities in ppm atomic of O, 190; N, 128; C, 34; F, 80; and Fe, 7.6. The metal was scraped free of any dark surface in the box before pieces were cut and weighed. Electropolishing was not carried out in order to reduce adventitious C, F, and O values. The electronic grade Ge (Johnson-Matthey) had a reported ρ_{293} value of 50 Ω cm. The other reactants utilized were as follows: B (99.5%) and Co (3–9's), Aesar; C (spec-grade), Union Carbide; La_2O_3 (five 9's), Ames Lab; P (five 9's) and As (six 9's), Aldrich; Sb (reagent), Allied Chemical; S (five 9's), Alfa; Se (five 9's), American Smelting & Refining; Bi (reactor grade), Oak Ridge National Lab; Te (five 9's), United Mineral & Chemical; Zn and V (four 9's), Fisher Scientific; Cd (five 9's), Cominco Products; Mn (three 9's), Cr (three 9's 5), A. D. Mackay; Fe (three 9's), Plastic Metals; Ni (reagent), Matheson, Colman & Bell; Cu (four 9's), J. T. Baker; Ru (three 9's 5), Engelhard. Sublimed $LaCl_3$ and LaN were prepared in house as sources of those nonmetals.

Syntheses. Tantalum proved to be a satisfactory container for all of the systems described here. It was cleaned and welded as before.[9,14] Post-reaction ductility of this container is a good indication that it has not been attacked since a reaction usually results in precipitation of a tantalum compound at the grain boundaries.

Reactions at $T \leq 1050$ °C were usually carried out with the tantalum container jacketed in well-baked, evacuated, and sealed SiO_2 tubing. Those at higher temperatures were usually run with the bare Ta container in the high temperature vacuum furnace described earlier.[14,34] Quenched samples from the higher temperature region were obtained following induction heating. Many of the reactions were carried out starting with pressed pellets of finely ground elements or prereacted binary phases that had been selected for their brittleness (e.g., LaP, LaAs). The grinding–pelleting–sintering cycle was repeated if necessary to gain homogeneity. A few arc-melting reactions following Zr gettering were used with the recognition that such products are susceptible to contamination, mainly from oxygen and nitrogen, and that they are also apt to provide inhomogenous samples and disordered structures.[14,35] Annealing in Ta was subsequently used to alleviate the last problem. With all of these methods, the production of a single phase product (according to Guinier diffraction) with distinctive and reproducible dimensions was taken as indicative of the formation of a stoichiometric La_5Ge_3Z compound.

Property Measurement. A JEOL JSM-840 SEM equipped with a KEVEX EDX system was used for some elemental analyses. Qualitative checks were also routinely carried out on new synthetic products. Quantitative studies were made on well-facetted crystals fixed in epoxy, polished with sandpaper and leather, and grounded to the copper holder with silver paint. Samples were examined in the back-scattering and topological modes to select sites for analysis. The bulk compositions were used for standards whenever possible to avoid matrix errors.

Magnetic susceptibilities were measured between 6 and 300 K on a MPMS SQUID instrument from Quantum Design, usually at 3 T. An improved container was designed in which the sample is held between the flat faces of two 3-mm-diameter SiO_2 rods.[33,36]

Electrical resistivity properties were estimated in the glovebox on large chunks or pressed pellets with the aid of a commercial multimeter. Better values were measured over a 100–300 K range by the "Q" method[37] on sized (150–250 μm) samples mixed with silica powder. Data were also obtained for La_5Ge_3 over 83–293 K with the aid of a four-probe apparatus.[38]

X-ray Studies. Guinier powder pattern techniques, lattice constant measurement methodology therefrom, and program packages have been described before.[14] Single crystal studies were carried out on La_5Ge_3 and La_5Ge_3Cr. A gemlike crystal of the former was examined with oscillation photographs and then a 2-fold redundant data set was collected on a DATEX instrument up to $2\theta = 55°$ with the aid of Mo Kα radiation. Reflection data corrected for absorption with the aid of θ-dependent ψ-scan data gave $R_{av} = 2.6\%$ for observed data. Use of the atom positions from the parent structure resulted in rapid convergence and a well-behaved result. An SEM analysis gave the composition $La_5Ge_{3.04(1)}$.

The same diffractometer, octants, and limits were employed for data collection on La_5Ge_3Cr crystal obtained from a sintering reaction. Axial (polaroid) and Weissenberg photographs confirmed the Laue class and lattice parameters. ψ-scans were again applied to correct for absorption, providing $R_{av} = 2.8\%$ for data with $I/\sigma_I > 3$. An uneventful refinement, with Cr deduced in a ΔF map, provided a clear result. A refined stoichiometry of $La_{4.99(1)}Ge_{3.02(1)}Cr_{0.97(2)}$ (La1 fixed) agreed well with the ideal model. Some collection and refinement data for both studies are given in Table I.

(17) Hurng, W.-M.; Corbett, J. D. *Chem. Mater.* **1989**, *1*, 311.
(18) Leon-Escamilla, E. A.; Corbett, J. D. Unpublished research.
(19) Al-Shahery, G. Y. M.; Jones, D. W.; McColm, I. J.; Steadman, R. *J. Less-Common Met.* **1982**, *85*, 233.
(20) Al-Shahery, G. Y. M.; Jones, D. W.; McColm, I. J.; Steadman, R. *J. Less-Common Met.* **1982**, *87*, 99.
(21) Al-Shahery, G. Y. M.; McColm, I. J. *J. Less-Common Met.* **1983**, *92*, 329.
(22) Button, T. W.; McColm, I. J. *J. Less-Common Met.* **1984**, *97*, 237.
(23) Mayer, I.; Shidlovsky, I. *Inorg. Chem.* **1969**, *8*, 1240.
(24) Eremenko, V. N.; Shi, Z. K.; Buyanov, Yu. I.; Kharkova, A. M. *Dokl. Akad. Nauk. Ukr. RSR* **1972**, *9*, 819–823.
(25) Nasibov, I. O.; Rustamov, P. G.; Alijeva, M. M. *Russ. Metall.* **1973**, *5*, 163.
(26) Gladyshevskii, E. I. *J. Struct. Chem. (Engl. Transl.)* **1964**, *5*, 852.
(27) Parthé, E.; Jeitschko, W.; Sagadopan, V. *Acta Crystallogr.* **1965**, *19*, 1031.
(28) Arbuckle, J.; Parthé, E. *Acta Crystallogr.* **1962**, *15*, 1205.
(29) Buschow, K. H. J.; Fast, J. F. *Phys. Status Solidi* **1967**, *21*, 593.
(30) Lyutaya, M. D.; Goncharuk, A. B. *Inorg. Mater.* **1965**, *1*, 302.
(31) Lynchak, K. A.; Kosolapova, T. Ya. *Poroshk. Met. (Kiev)* **1967**, 92.
(32) Lynchak, K. A.; Kosolapova, T. Ya.; Kuz'ma, Yu. B. *Porosh. Met. (Kiev)* **1968**, 54.
(33) Guloy, A. M.; Corbett, J. D. To be submitted for publication.
(34) Guloy, A. M.; Corbett, J. D. *Inorg. Chem.* **1991**, *30*, 4789.
(35) Kwon, Y.-U.; Corbett, J. D. *Chem. Mater.* **1990**, *2*, 27.
(36) Sevov, S. C.; Corbett, J. D. *Inorg. Chem.* **1992**, *31*, 1895.
(37) Shinar, J.; Dehner, B.; Beaudry, B. J.; Peterson, D. T. *Phys. Rev. B* **1988**, *37*, 2066.
(38) Wolfe, L. G.; Corbett, J. D. Unpublished research.

Table I. Data Collection and Refinement Parameters for La_5Ge_3 and La_5Ge_3P

	La_5Ge_3	La_5Ge_3Cr
space group; Z	$P6_3/mcm$ (No. 193); 2	$P6_3/mcm$ (No. 193); 2
cell params[a]		
a, Å	8.9409 (5)	9.0043 (7)
c, Å	6.8784 (6)	7.1048 (8)
V, Å^3	476.19 (9)	498.86 (8)
no. of indep reflcns; no. of variables	270, 12	278, 14
abs coeff, cm^{-1} (Mo Kα)	312	342
R_{av}, % (obsd data)	2.6	2.8
R,[b] %	3.4	2.4
R_w,[c] %	3.8	2.9

[a] Guinier data with Si as internal standard, λ = 1.540 592 Å. [b] $R = \sum||F_o| - |F_c||/\sum|F_o|$. [c] $R_w = [\sum w(|F_o| - |F_c|)^2/\sum w(F_o)^2]^{1/2}$; $w = \sigma_F^{-2}$.

Table II. La-Ge System: Phases, Structure Types, and Lattice Parameters (Å)[a]

composition	struct type (space group)	a	b	c
La_3Ge	Ti_3P ($P4_2/n$)	12.741(2)		6.298(1)
La_5Ge_3	Mn_5Si_3 ($P6_3/mcm$)	8.941(1)		6.878(1)
La_4Ge_3	Th_4P_3 ($I\bar{4}3d$)	9.3548(3)		
La_5Ge_4	Sm_5Ge_4 ($Pnma$)	8.065(1)	15.474(2)	8.172(1)
LaGe	FeB ($Pnma$?[b])	8.488(1)	4.128(1)	6.122(1)
$LaGe_{1.60}$[c]	α-$GdSi_2$ ($Imma$)	4.2680(7)	4.2735(6)	14.404(1)

[a] Room temperature Guinier data. [b] See text. [c] Reference 34.

Extended-Hückel band structure calculations were carried out for La_5Ge_3, La_5Ge_3P, and La_5Ge_3Fe using a standard program[39] modified as to capacity and with the addition of symmetry elements.[40] A total of 60 and 90 k points were used for DOS and POP plots, and 36 were used for band analysis. Literature parameters were utilized for La, Ge, and P while H_{ii} data for Fe were charged-iterated values obtained from an idealized La_3Fe structure (a $La_{6/2}Fe$ chain of face-sharing octahedra) with the same distances as in $La_{15}Ge_9Fe$ (H_{ii} (s,p,d) = −7.75, −3.75, −9.36 eV, respectively).

Results and Discussion

La–Ge System. The binary system was surveyed in the course of this and other studies to establish the identity of all phases. Those listed in the most recent phase diagram summary[41] were confirmed as well as the space groups of all but two, Table II. The Guinier pattern of the metal-richest and previously structurally uncharacterized phase La_3Ge was found to be that of a tetragonal Ti_3P-type structure with the indicated parameters. Single crystal data were refined for La_5Ge_3 (below), for La_4Ge_3 as part of another investigation,[33] and for $LaGe_{1.60}$ as already published.[34] However, the FeB structure previously assigned to LaGe may not be correct in all detail. Three very weak extra lines appeared in the powder pattern, and their intensities in mixtures seemed to parallel those of other weak lines from the assigned structure. This implies that some symmetry-reducing transition may be involved; a metal-to-semiconductor polymorphic transition has been reported to occur in LaGe at 440 °C.[42] Further studies were not attempted because of our inability to grow suitable monocrystals.

The host La_5Ge_3 was established as substantially a line phase following equilibration of samples over the composition range of $La_5Ge_{2.5}$ to $La_5Ge_{3.25}$. Methods included melting the elements at 1250 °C followed by slow cooling or annealing at 800 °C, quenching from 1400 °C in an induction coil, and arc melting. The La_5Ge_3 phase throughout showed only very slight increases in lattice constants with increasing Ge content, the extremes being 3.5σ and 4σ in Δa and Δc, respectively. On the other hand, these dimensional data show significant differences from most, but not all, literature values, including for a reported La_5Ge_3 product of a germaniothermal reaction, viz., $5La_2O_3 + 21Ge \rightarrow 2La_5Ge_3 + 15GeO(g)$.[30] On the basis of our experiences with other systems of the same structure type, such divergences are commonly caused by impurities, particularly the common nonmetals.[13-16] Therefore, their effects were systematically investigated starting with the nonmetals O, C, B, and N in that order.

Oxygen. Single-phase samples of La_5Ge_3O were obtained by either sintering pressed pellets of La, Ge, and La_2O_3, or by arc melting of the same components. Some results are summarized in Table III. A distinctive (but small) increase in the a dimension and a greater contraction in c with an overall decrease in volume are characteristic of small interstitials in this structure type.[14-16] A lesser oxygen fraction leads to the appearance of a new $La_{15}Ge_9Fe$-type phase $La_{15}Ge_9O$ with a $\sqrt{3} \times \sqrt{3} \times 1$ ordered superstructure ($P6_3/mc$) that will be described in detail in a separate publication.[33] This phase is evidenced by only a few weak lines ($I/I(\max) \leq 0.04$) in the Guinier pattern. No other phases appear in the quasi-binary system (short of La_2O_3), in particular no analogue of the stuffed Cr_5B_3 version found for La_5Pb_3O.[43] Broadening of the strongest of the substructure lines in mixtures with either La_5Ge_3 or La_5Ge_3O may result from the close similarity of their dimensions, or it may mean that more is happening than we appreciate. The principal lattice dimension variations of the two oxides from La_5Ge_3 is the ~0.12 Å contraction in c, while La_5Ge_3O and $La_{15}Ge_9O$ ($a = (\sqrt{3})(8.969(1))$, c = 6.758(1) Å) cannot be distinguished from each other by their (sub)lattice dimensions. Both appear to be particularly air stable, for weeks at room temperature visually.

The c dimensions of the oxides are virtually identical to those reported for the presumed La_5Ge_3 by Gladyshevskii[26] following element fusion and by Arbuckle and Parthé[28] after arc-melting. Handling lanthanum for any period of time in the air could have been responsible, as is clearly true for La_5Sn_3O since pure La_5Sn_3 does not have this structure.[13] On the other hand, the diagnostic dimensions for La_5Ge_3 reported by Mayer and Shidlovsky[23] and, particularly, by Buschow and Fast[29] are identical to ours within the indicated precisions (Table II). It seems clear that the unusual germaniothermal synthesis of La_5Ge_3 claimed by Lyutaya and Goncharuk[28] in fact gives the oxide, probably La_5Ge_3O judging from the reduced c dimension. This is especially supported by their statement, and those of others,[26,28] that La_5Ge_3 is virtually air stable; we observe it to be quite sensitive to moist air, decomposing in bulk in less than an hour or as a powder in 10–15 min. The synthesis of tetragonal $LaGe_2$ by the appropriate reaction of La_2O_3 and Ge was also reported. We have earlier found that the high temperature tetragonal structure type for $LaGe_2$ is stabilized at room temperature by a small amount of oxygen.[34] The previous reactions thus should evidently be formulated as

$$5La_2O_3 + 19Ge \rightarrow 2La_5Ge_3O + 13GeO(g)$$

and

$$La_2O_3 + (7 - 2x)Ge \rightarrow 2LaGe_2O_x + (3 - 2x)GeO(g)$$

Similar syntheses from R_2O_3 have been reported for Pr_5Ge_3 and Nd_5Ge_3[31,32] and also for analogous RSi_{2-x} phases in both the tetragonal and orthorhombic structures.[44]

Carbon. The carbide $La_5Ge_3C_x$ apparently obtained from sintering reactions at 1250 °C shows fixed lattice constants (Table IV) over the range $0.85 \leq x < 1.25$ that are somewhat larger than

(39) Whangbo, M.-H.; Hoffmann, R.; Woodward, R. B. *Proc. R. Soc. London* **1979**, *A366*, 23.
(40) Kertesz, M. Personal communication, 1989.
(41) Gokhale, A. B.; Abbaschian, G. J. *Bull. Alloy Phase Diagrams* **1989**, *10*, 385.
(42) Rud, B. M.; Lynchak, K. A.; Paderno, Yu. B. *Sov. Powder Metall. Met. Ceram.* **1968**, *72*, 216.
(43) Guloy, A. M.; Corbett, J. D. *Z. Anorg. Allg. Chem.* **1992**, *616*, 61.
(44) Perri, J. A.; Binder, I.; Post, B. *J. Phys. Chem.* **1959**, *63*, 616.

Table III. Summary of La_5Ge_3-O Reactions and Literature Comparisons

reaction or reported composition	conditions[a]	struct type of products[b]	a[c]	c	c/a	assignt
La_5Ge_3	S	M	8.941 (1)	6.878 (1)	0.769	La_5Ge_3
La_5Ge_3O	S	M	8.957 (1)	6.759 (1)	0.755	La_5Ge_3O
La_5Ge_3O	A	M	8.962 (2)	6.766 (1)	0.755	La_5Ge_3O
$La_5Ge_3O_{0.75}$	S	M + S	8.956 (2)	6.762 (2)	0.755	$La_5Ge_3O + La_{15}Ge_9O$
$La_5Ge_3O_{0.50}$	S	M + S	15.537 (1)	6.760 (2)	$0.754/\sqrt{3}$	$La_5Ge_3O + La_{15}Ge_9O$
$La_5Ge_3O_{0.33}$	S	S	15.535 (1)	6.758 (1)	$0.754/\sqrt{3}$	$La_{15}Ge_9O$
La_5Ge_3[d]	A	M	8.96 (1)	6.74 (1)	0.752	La_5Ge_3O or $La_{15}Ge_9O$
La_5Ge_3[e]	F	M	8.96 (1)	6.74 (1)	0.752	La_5Ge_3O or $La_{15}Ge_9O$
La_5Ge_3[f]	Ge't	M	8.97 (1)	6.76 (1)	0.754	La_5Ge_3O
La_5Ge_3[g]	A, An	M	8.930	6.874	0.770	La_5Ge_3
La_5Ge_3[h]	I	M	8.95 (1)	6.90 (1)	0.771	La_5Ge_3

[a] Key: S, reactive sintering at 1250 °C for 3–5 d; A, arc-melting; F, fusion of elements at 1300 °C in ThO_2; Ge't, germaniothermal reaction (see text); I, induction heating at 1500 °C; An, annealing at 700–900 °C. [b] Key: M, Mn_5Si_3 type; S, $La_{15}Ge_9Fe$ type. [c] Data for major phase if in mixture. [d] Reference 28. [e] Reference 26. [f] Reference 30. [g] Reference 29. [h] Reference 23.

Table IV. Dimensions of La_5Ge_3 and La_5Ge_3Z[a]

	synth method[b]	a	c	V	c/a
La_5Ge_3	M	8.941(1)	6.878(1)	476.2(1)	0.769
La_5Ge_3O	S	8.957(1)	6.759(1)	469.6(1)	0.755
La_5Ge_3N	S	8.959(1)	6.761(1)	470.0(1)	0.755
$La_5Ge_3C_x$[c]	S	8.955(1)	6.904(1)	479.5(1)	0.771
$La_5Ge_3B_x$[c]	S	8.970(1)	6.915(1)	481.8(1)	0.770
La_5Ge_3P	SB	8.980(1)	6.982(1)	487.6(1)	0.778
La_5Ge_3As	SB	9.104(1)	7.121(1)	511.0(1)	0.782
La_5Ge_3Sb	S	9.156(1)	7.231(1)	525.0(1)	0.790
La_5Ge_3S	SB	8.992(1)	7.031(1)	492.3(1)	0.782
La_5Ge_3Se	SB	9.112(1)	7.161(1)	515.0(1)	0.786
La_5Ge_3Cl	SB	8.955(1)	6.897(2)	495.3(1)	0.781
La_5Ge_3Cr	S	9.004(1)	7.105(1)	498.8(1)	0.789
La_5Ge_3Mn	S	8.969(1)	7.104(1)	494.9(1)	0.792
La_5Ge_3Fe	I	8.956(1)	7.080(1)	491.5(1)	0.790
La_5Ge_3Co	S	8.956(1)	7.101(1)	493.2(1)	0.792
La_5Ge_3Ni	S	8.950(1)	7.042(1)	488.5(1)	0.787
La_5Ge_3Cu	S′	8.989(1)	7.112(1)	497.2(1)	0.791
La_5Ge_3Zn	S′	9.025(1)	7.185(1)	506.8(1)	0.796
La_5Ge_3Cd	S′	9.108(1)	7.152(2)	513.8(1)	0.785
La_5Ge_3Ru	S	9.024(1)	7.121(1)	502.2(1)	0.789

[a] Guinier data for hexagonal cells, $P6_3/mmc$. [b] Key: M, fusion of elements; S, sintered pellet of powdered elements at 1250 – 1350 °C for 10–15 d; SB, sintered binary compounds in pellet, slowly heated to 1200 °C and annealed at 1000 °C over 10 days total; I, induction heated at 1400 °C; S′, same as S but with SB temperature routine. [c] See text regarding stoichiometry.

those of La_5Ge_3. However, LaC_2 was also always seen for $x \geq 1$. With decreasing x these dimensions appear to decrease by 5σ and 6.7σ (to a = 8.948 (1) Å and c = 6.887 (2) Å) at x = 0.50 where a $La_5Ge_3C_x$ phase in equilibrium with $La_{15}Ge_9C$ is observed. Formation of the latter is signaled not just by the extra lines but also by smaller dimensions ($(\sqrt{3})(8.9301\ (4))$, 6.880 (1) Å) that are closer to those of the empty binary. Only the superstructure phase, with fixed lattice constants, can be discerned at x = 0.25 and 0.33, and the composition $La_{15}Ge_9C$ (x = 0.33) has been well confirmed by single-crystal X-ray studies.[33]

The above observations suggest that the carbon-richer phase has $0.7 < x < 1.0$. This is not out of reason as far as the expectation of a limit of $La_5Ge_3C_{0.75}$ for a valence (Zintl) phase. Beyond this, either LaC_2, etc., or holes in the low-lying valence band of Ge (or C) should form. A change of structure type in the latter case to allow for nonmetal dimerization would be expected based on our other studies of La_5Tt_4 systems (Tt = tetregen).[33] (Products with Al, Ga, In also fall in this category). Our synthesis and powder diffraction techniques are obviously limited in their ability to define the composition of the higher carbide more accurately. On the other hand, the expected behavior is clearly seen in the analogous $La_5Ge_3Si_x$ system where a single Mn_5Si_3-type, high temperature phase is present at x = 0.75, while diverse structures that contain Ge(Si) dimers form for greater x values. Two such carbide examples were also seen at greater extremes ($x \geq 1.5$), an Sm_5Ge_4-type phase and $La_5Ge_2C_2$, which is related to the Rh_5Ge_3 type.[33]

Several nominally stoichiometric R_5Si_3C and R_5Ge_3C products have been reported in this structure type.[23] A $\sqrt{3} \times \sqrt{3} \times 1$ superstructure has been observed for substoichiometric $R_5Si_3C_x$ (R = Y, Gd, Ho, Er),[19-22] but compositional or structural details were not established. We find La_5Si_3 is Cr_5B_3 type, as reported before,[45] but this converts to a stuffed Mn_5Si_3-type as La_5Si_3O, a = 8.864(2) Å, c = 6.718(2) Å. The lattice dimensions reported for a possible Mn_5Si_3 type of La_5Si_3[46] seem much too large even with interstitials. La_5Sn_3 (W_5Si_3 type) gives similar results to La_5Ge_3 with carbon (above), a = 9.396 (2) Å, c = 6.934 (1) Å at x = 0.75, c being 9σ larger at x = 1.0 with no other phases evident. At x = 0.5 only $La_{15}Sn_9C$ was seen.

Boron, like carbon, produces an expansion of the host lattice. Significant phase breadth is indicated by the equilibration results for $0.25 \leq x \leq 1.25$, all of which gave single phase products by Guinier powder diffraction. Cell parameters of $La_5Ge_3B_x$ increase regularly but *modestly* with boron content, from 8.941(1) and 6.880(2) Å at $x \sim 0.3$, nearly equal to those for La_5Ge_3, to 8.970(1) and 6.916(1) Å near x = 0.75 (20σ and 14σ changes). No superstructure was seen. A poorly crystalline LaB_x must have formed for $x > 0.75$ where the measured dimensions appeared to be constant. Zintl concepts would predict a limiting composition $La_5Ge_3B_{0.60}$ for a valence compound, whereas our X-ray dimensional data suggest a terminus somewhere in the range $0.6 \leq x \leq 0.8$. The lattice dimensional changes are in any case small, so stoichiometric conclusions are not too firm, but a modest contradiction of simple valence ideas may be possible. These changes were not resolved (at ±0.01 Å) in an early study by Mayer and Felner,[47] a possible small decrease only in c perhaps resulting from contamination.

Nitride syntheses were readily accomplished by slowly heating a pressed pellet of LaN plus the elements to 1050–1150 °C followed by slow cooling.

Pnictogens (Pn) give valence-precise La_5Ge_3Pn products. Single-phase materials were obtained for Pn = P, As, Sb (Table III) but not for Bi, which gave multiple products that were not explored further. Semiquantitative SEM analyses of individual (unpolished) crystals gave $La_5Ge_{2.97(5)}P_{1.1(3)}$, $La_5Ge_{3.0(1)}As_{0.9(1)}$, and $La_5Ge_{3.0(2)}Sb_{0.95(5)}$. The superstructure was also found with phosphorus. These products have distinctive appearances, dull black in contrast to the metallic luster presented by La_5Ge_3. The first was shown to be a semiconductor (below).

Chalcogen and halogen products were also achieved with S, Se, and Cl. Use of prereacted binary lanthanum phases for S, Se, and Cl (as well as for P and As above) avoided the problems that the elements would engender in tantalum containers. Reactions

(45) Smith, G. S.; Tharp, A. G.; Johnson, Q. *Acta Crystallogr.* **1967**, *22*, 940.
(46) Dvorina, L. A.; Verkhoglyadova, T. S. *Russ. Metall.* **1965**, *6*, 38.
(47) Mayer, I.; Felner, I. *J. Less-Common Met.* **1974**, *37*, 171.

with Te and I produced only other unknown phases. The three weak lines from LaOCl that also appeared in the pattern for the chloride suggest that this may provide a method to remove oxide from La_5Ge_3O as chloride does from the metals.[48]

Transition metals afforded a broader range of bound Z than has been achieved in several Zr_5M_3 hosts. Synthetic and dimensional details for Z = Cr, Mn, Fe, Co, Ni, Cu, and Ru as well as for Zn and Cd appear in Table III. On the other hand, incorporation of Ti or V was not successful. Arc-melted products characteristically gave more diffuse patterns and lattice parameters that were consistently >0.02 Å larger. The related $La_{15}Ge_9Z$ phases were identified for Z = Mn, Fe, Co, Ni, Cu, and Ru, but were not found for Zn or Cd.[33] Lattice constants of La_5Ge_3Z products in equilibrium with the superstructure phase were nearly identical with those found for pure La_5Ge_3Z, Z = Mn, Co, and Ni, indicating that the filled members are substantially line phases.

Only iron among these new examples gave any trouble. The phase La_5Ge_3Fe was inferred from the fixed lattice dimension increase, SEM examinations, XPS data and its distinctive ferromagnetism.[33] Single phase samples were obtained on quenching from above 1350 °C, generally after arc melting or induction heating at 1400 °C in Mo-lined Ta containers. Some disorder between Fe and Ge sites cannot be ruled out. Slow cooling in Ta with or without a Mo lining led to decomposition into $La_{15}Ge_9Fe$ and a second phase that could be completely indexed as the *bcc* structure known for La_4Ge_3 (*anti*-Th_3P_4, $I\bar{4}3d$, a = 9.414(4) vs 9.3548(3) Å for the binary, Table II). SEM analyses of the second phase were in the neighborhood of $La_4Ge_{2.3}Fe$ with a range of $La_4Ge_{2.0}Fe_{1.3}$ to $La_4Ge_{2.8}Fe_{0.6}$. Any iron that was lost was found qualitatively in the Ta container. (The phase diagram shows Fe solution in Ta even at 800 °C,[49] a process that has also troubled us elsewhere.[50]) By implication, the Th_3P_4-type structure not only has Fe substitution on Ge sites, as previously seen for R_4Bi_{3+x} phases,[51] but also excess iron above 3/4 La (~0.3) in tetrahedral interstitial sites. The latter is known in $Y_3Au_3Sb_3$[52] and has also been found for Ru in $La_4Ge_{2.25}Ru_{1.1}$.[33]

Crystal Structure Studies. These were carried out for La_5Ge_3, both to gain metric details and to show that the interstitial site was indeed empty, and for La_5Ge_3Cr, which represents the first incorporation of this element into an Mn_5Si_3-type host. The positional parameters for both appear in Table IV, and some important distances and angles, in Table V. A separate publication will report crystal structural results for $La_{15}Ge_9Z$, Z = C, P, Mn, Fe, Co, Ni.[33] Figure 1 shows a [001] projection of the La_5Ge_3 result at the top and a partial [110] section of the two chains in La_5Ge_3Cr at the bottom. The metal atoms comprising the linear La1 chain do not appear to enter into this type of chemistry readily.

The La_5Ge_3 is evidently stoichiometric with the so-called interstitial site empty. The La2 and Ge sites relative to La1 refined to unity within 1 and 2% (1.2σ and 2.5σ), respectively, while the residual in the center of the cavity ($\bar{3}$m) was 1.6 e$^-$/Å^3. Only hydrogen would be possible as an interstitial, and although this is known to bind in analogous alkaline-earth-metal systems,[18] it is very unlikely here since the synthesis and crystal growth took place under high vacuum (induction heating) conditions (mp 1475 °C).

The new La_5Ge_3Cr has the expected structure and appears to be fully stoichiometric. This represents the second time Cr has been inserted inside any cluster, the only other example being

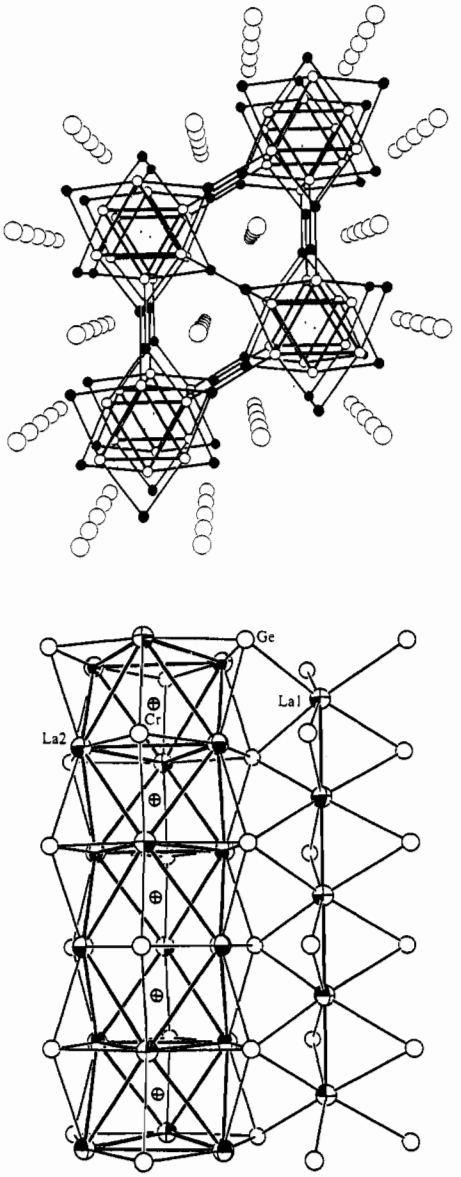

Figure 1. Top: [001] projection of the structure of La_5Ge_3 (Mn_5Si_3-type, $P6_3/mcm$). Open (90%) ellipsoids are La; solid ellipsoids are Ge. The atoms shown isolated are La1. The interstitial sites are marked with small dots. Bottom: Partial [110] section of the La_5Ge_3Cr structure showing, left, the confacial chains of La2 (shaded) atoms centered by Cr (crossed) and, right, the linear chain of La1 (c axis vertical). The two chains are interconnected by common germanium atoms. (Idealized ellipsoids).

$Zr_6I_{12}Cr$.[53] This infrequency probably says more about the relative stabilities of alternate phases of chromium than anything about intrinsically good or poor bonding of Cr in these hosts. No other phases with La–Cr bonding are known for comparison, but an uncritical summation of Pauling's single bond metallic radii[54] gives 2.876 Å, not too far above the observed 2.801(1) Å. This latter gives the impression of appreciable La–Cr bond strength (at least as reflected by distance) since the formal bond order even in an isolated cluster is only 0.67 ($a_{1g} + t_{2g}$[53]). The Zr–Mn and Zr–Fe bond lengths in isolated Zr_6Cl_{12}-type clusters with more anisotropic environments around the M_6Z unit are generally 0.20–0.23 Å *less* than the comparable single-bond radius sums.[55] Differences for the corresponding $La_{15}Ge_9Z$ (Z = Mn–Ni) phases

(48) Corbett, J. D.; Smith, J. D.; Garcia, E. *J. Less-Common Met.* **1986**, *115*, 343.
(49) Swartzendruber, L. J.; Paul, E. In *Binary Alloy Phase Diagrams*; Massalski, T. B., Ed.; ASM International: Materials Park, OH, 1990; Vol. 2, p 1776.
(50) Kwon, Y.-U.; Sevov, S. C.; Corbett, J. D. *Chem. Mater.* **1990**, *2*, 550.
(51) Carter, F. L. *J. Solid State Chem.* **1972**, *5*, 300.
(52) Hyde, B. G.; Andersson, S. *Inorganic Crystal Structures*; John Wiley and Sons: New York, New York, 1989, p 335.
(53) Hughbanks, T.; Rosenthal, G.; Corbett, J. D. *J. Am. Chem. Soc.* **1988**, *110*, 1511.
(54) Pauling, L. *Nature of the Chemical Bond*; Cornell Press: New York, 1960; p 400.
(55) Zhang, J.; Corbett, J. D. *Inorg. Chem.* **1991**, *30*, 431.

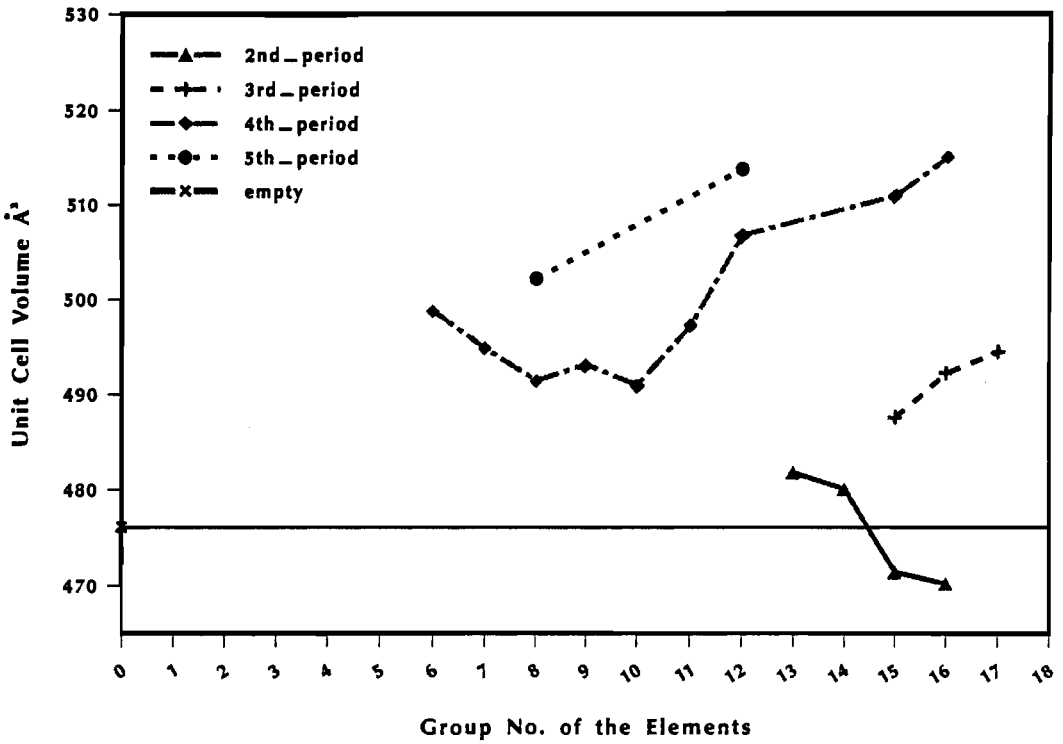

Figure 2. Unit cell volumes (Å³) of La_5Ge_3Z as a function of period and group of Z. The horizontal line marks the volume of the La_5Ge_3 host.

Table V. Positional Parameters[a] and Important Distances (Å) and Angles (deg) for La_5Ge_3 and La_5Ge_3Cr

Positional Parameters

	La_5Ge_3			La_5Ge_3Cr		
	x	occup[b]	B_{eq},[c] Å	x	occup[b]	B_{eq},[c] Å²
La1	1/3	1	1.98(2)	1/3	1	1.94(2)
La2	0.2399(1)	0.990(8)	1.94(2)	0.2405(1)	0.990(8)	1.88(2)
Ge	0.6007(2)	0.980(8)	2.11(3)	0.6048(2)	1.02(1)	2.05(3)
Cr				0	0.97(2)	2.77(4)

Distances and Angles

	La_5Ge_3	La_5Ge_3Cr		La_5Ge_3	La_5Ge_3Cr
		Distances			
La1–Ge (6×)	3.2894(4)	3.2866(4)	La1–La1 (2×)	3.4392(4)	3.5524(4)
La2–Ge (2×)[d]	3.113(1)	3.106(2)	La1–La2 (6×)	3.876(1)	3.921(1)
La2–Ge (2×)	3.7228(9)	3.816(2)	La2–La2 (2×)[d]	3.715(1)	3.751(1)
La2–Ge (1×)	3.226(1)	3.280(1)	La2–La2 (4×)	4.053(1)	4.160(1)
La2–Z (6×)	(2.749(1))	2.801(1)	Cr–Cr (2×)		3.5524(4)
		Angles			
La2–La2–La2	149.31(2)	149.83(2)	La2–Cr–La2		84.07(4)
La2–Ge–La2	72.11(3)	73.08(3)	La2–Cr–La2		95.93(4)
La1–Ge–La1	64.35(1)	65.43(1)			
La1–Ge–La1	147.62(4)	146.63(4)			
La1–Ge–La2	73.81(2)	73.32(2)			
Ge–La1–Ge	161.80(4)	161.80(4)			

[a] $P6_3/mcm$; La1 at 1/3, 2/3, 0; La2 at x, 0, 1/4; Ge at x, 0, 1/4; Cr at 0, 0, 0. [b] Reset to unity in final cycle. [c] $B_{eq} = (8\pi^2/3)\sum_i\sum_j U_{ij}a_i^*a_j^*\vec{a}_i\vec{a}_j$. [d] Perpendicular to $\vec{c}$.

are in the same direction by ~0.16–0.19 Å,[33] these phases being electron-richer than the analogous La_5Ge_3Z.

Interstitial Generalities. These La_5Ge_3Z systems provide new perspectives and generalities regarding the many stuffed Mn_5Si_3Z-type systems possible. Previous extensive investigations have dealt with the zirconium-based Zr_5Sb_3, Zr_5Sn_3, and Zr_5Pb_3 hosts and, in a more limited way, with the Ae_5Pn_3 systems (Ae = Ca, Sr, Ba; Pn = Sb, Bi) where only Z = Cl, Br, and H are bound, for electronic and size reasons.[14-18] The three zirconium systems are relatively similar to one another as far as the lists of Z that may be bonded, perhaps because of their common Zr_6Z structural unit, but with a somewhat greater variety in Zr_5Pb_3, possibly because of the host's greater size.

The variety of Z possible in La_5Ge_3Z

								B_x	C_x	N	O	
Cr	Mn	Fe	Co	Ni	Cu	Zn			$Si_{3/4}$	P	S	Cl
		Ru				Cd				As	Se	
										Sb		

is somewhat broader than found for zirconium examples and includes both Cr and Cl as extremes. On the other hand, the more limited number of valence electrons available in the empty host, 3 vs 8–11, appears to preclude stoichiometric La_5Ge_3Z examples in this structure for members of the Al and Si families, evidently because of the greater valence electron requirements of these interstitials. However, a fractional content of bound B and C seems likely (nominally 0.6 and 0.75), but this quantity could not be well defined by present methods (see above).

The lower conduction electron count of lanthanum is reflected in a distinctly higher c/a ratio in La_5Ge_3 and, correspondingly, a more elongated trigonal antiprism about the empty Z site. The effect is general; the above zirconium binaries have c/a = 0.683–0.685, which increases to 0.732 in La_5Pb_3, 0.769 for La_5Ge_3, and 0.778–0.781 for Ae_5Pn_3. The size of the Ae cation in the last series has a very small effect on the ratio although it naturally influences lattice dimensions and d(Ae–Z). Corresponding increases in the relatively short d(M1–M1) = $c/2$ along the linear chain in these hosts also follow the decrease in conduction electron count, which naturally goes to zero in ternary Zintl phases like La_5Ge_3Pn (below) and Ae_5Pn_3Cl.

Two general effects are evident on Z encapsulation. The more compressed antiprisms in the Zr_5M_3 compounds show particularly notable increases in c/a with the more negative pnictide and chalcogenide interstitials, presumably because of charge repulsions between neighboring members at $c/2 \leq 3.0$ Å. This effect is reduced in La_5Ge_3 and disappears in Ae_5Pn_3Cl where $c/2 = d$(Cl–Cl) ≥ 3.55 Å; instead, the cavity expands fairly uniformly on intercalation. The effects of Z encapsulation on cavity proportions change in parallel with c/a. The edges of the shared faces of the zirconium antiprisms expand about twice as much as do the side edges on forming Zr_5Sn_3(Ge,Ga) (by 0.40–0.46 vs 0.18–0.20 Å)[15] and Zr_5Sb_3(Si,Zn) (0.29–0.43 vs 0.10–0.17 Å),[14] in contrast

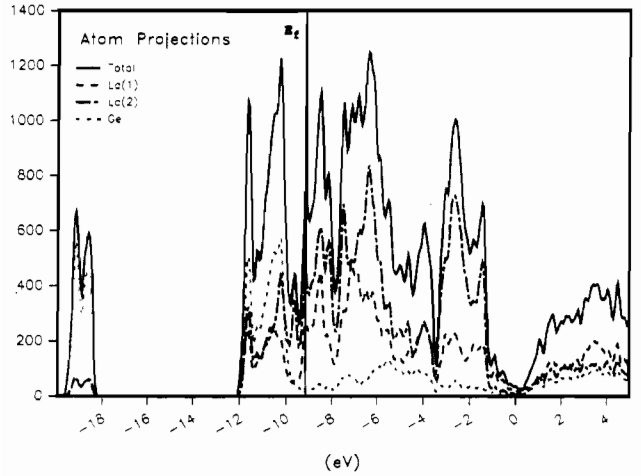

Figure 3. Total densities-of-states calculated for La_5Ge_3 (solid line) and the projection of atomic contributions for La1 (dashed), La2 in confacial chain (dash-dot), and Ge (light dashed).

Table VI. Data Derived from Extended-Hückel Calculations on La_5Ge_3 and La_5Ge_3Z

	La_5Ge_3	La_5Ge_3P	La_5Ge_3Fe
fermi energy (E_F), eV	−9.19	−9.38	−9.31
overlap populations			
La1–Ge	0.263	0.301	0.303
La2–Ge(ave)	0.296	0.263	0.258
La1–La1	0.100	0.088	0.060
La1–La2	0.101	0.042	0.036
La2–La2(xy)	−0.175	0.154	0.120
La2–La2(z)	0.190	0.041	0.031
La2–Z		0.191	0.187
Z–Z		−0.02	0.005
derived charges			
La1	+0.34	+0.40	+0.37
La2	+0.26	+0.63	+0.26
Ge	−0.49	−0.52	−0.47
Z		−1.12	−0.12

to the changes seen in the larger La_5Ge_3Cr, which are 0.04 and 0.11 Å, respectively.

The volume effects of Z in La_5Ge_3Z are illustrated in Figure 2 as a function of period and the group of Z, where the horizontal line marks the volume of the empty La_5Ge_3. Of course, cell parameter variations also contain the result of any changes in La2–Ge (inner and exo), La1–Ge and La2–La1 distances. The few single crystal results available indicate the latter changes are less substantial with the larger La_5Ge_3 than for Zr_5Sn_3, suggesting that the volume changes seen here more nearly reflect the partial volumes of Z. The volume contractions found for N, O also apply with carbon in Zr_5Sn_3 and Zr_5Sb_3, particularly with the latter, while the decrease in c/a is noteworthy in the present cases. The overall cell volume changes seen on insertion of a particular period two or three interstitial into La_5Ge_3 are comparable to those in analogous zirconium systems. However, the large and upward trend in volumes seen in Figure 2 along the fourth period is new. Increases in volume with the formation of Zr_5Sn_3Z and Zr_5Pb_3Z in particular are approximately constant for Z = Zn–Se (15–22 Å^3), well short of the 31–39-Å^3 increases for these in La_5Ge_3 (where comparable data are available). While the Zr_5Sn_3Z data in particular appear to parallel standard covalent/metallic radii fairly well, the notably greater expansions in La_5Ge_3Z within period 4 are hard to understand. They may arise from Coulombic effects in a more polar and less metallic host, although confirmatory dimensional data for pertinent examples are not available.

Properties. The electronic conduction properties of selected phases are consistent with our rather simple ways of accounting for electrons. Since the germanium atoms are isolated from one another in the Mn_5Si_3-type structure of La_5Ge_3, one would expect that four electrons from the metal will first fill the empty, low-lying valence levels of each germanium. (This does not, however, imply an ionic formulation.) Three electrons ($5 \times 3 - 3 \times 4$) then remain in a higher-lying conduction band, presumably largely lanthanum-based. The La_5Ge_3 host is suitably metallic, with room temperature resistivities measured by four-probe and "Q" methods of 25 and 90 μΩ cm and temperature dependencies of +0.73% and +0.95%, respectively. Furthermore, the forecasted Zintl phase La_5Ge_3P exhibited a resistivity at ~22 °C of ~580 μΩ cm by the "Q" method with a temperature coefficient of −0.98% and a band gap of ~0.11 eV. Qualitative two-probe (dc) measurements on the same phosphide in the glovebox at room temperature gave a resistivity of ~0.2 Ω, which of course included contact resistance. La_5Ge_3As gave a similar qualitative result.

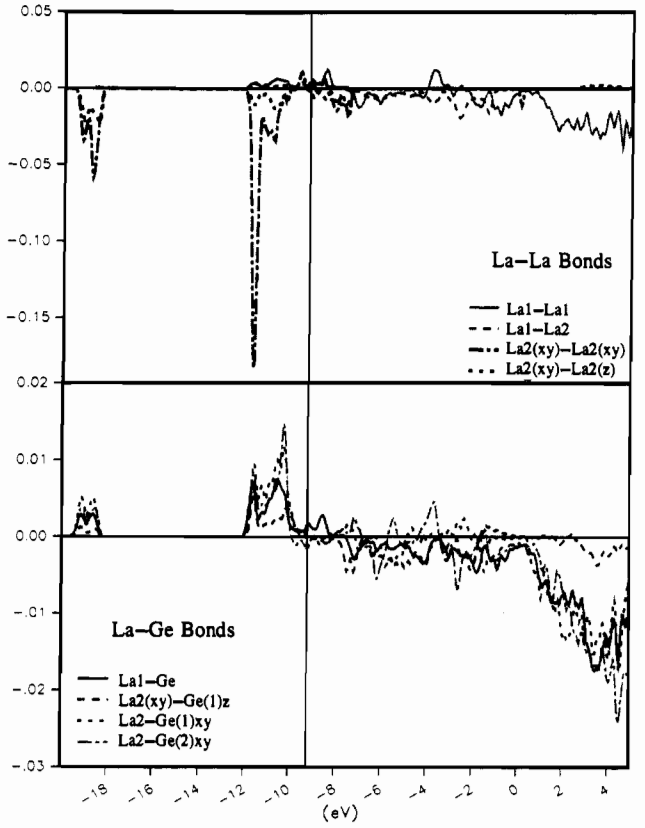

Figure 4. COOP curves for different types of La–La and La–Ge atom pairs in La_5Ge_3. Positive values are bonding (arbitrary abscissa scales). (xy and z distinguish La and Ge interactions perpendicular and parallel to the c-axis, respectively; La2–Ge(1) is edge-bridging, while La2–Ge(2) is exo between chains.)

Magnetic susceptibilities are in accord with the foregoing. La_5Ge_3 exhibits a Pauli-like 5.5×10^{-6} emu mol^{-1} (±5%) over the 100–300 K range after correction for core contributions. This confirms the qualitative report by Buschow and Fast.[28] In proper contrast, La_5Ge_3P is diamagnetic, $-8.3(4) \times 10^{-7}$ emu mol^{-1} after core corrections.

Band Calculations. Extended-Hückel calculations were carried out on La_5Gd_3, La_5Ge_3P, and La_5Ge_3Fe in order to gain additional understanding of their bonding and to compare the results with the qualitative electronic pictures implied by the foregoing. Some of the pertinent overlap populations and derived charges are summarized in Table VI.

The calculated band structure of La_5Ge_3 is represented in Figure 3 by the total density of states (top solid line) as well as the projections of the DOS for the three independent atoms (La2 defines the confacial chain). The low lying band at the far left is largely Ge 4s mixed with a small amount of La, while that in the region between −12.0 and −9.7 eV contains the principal

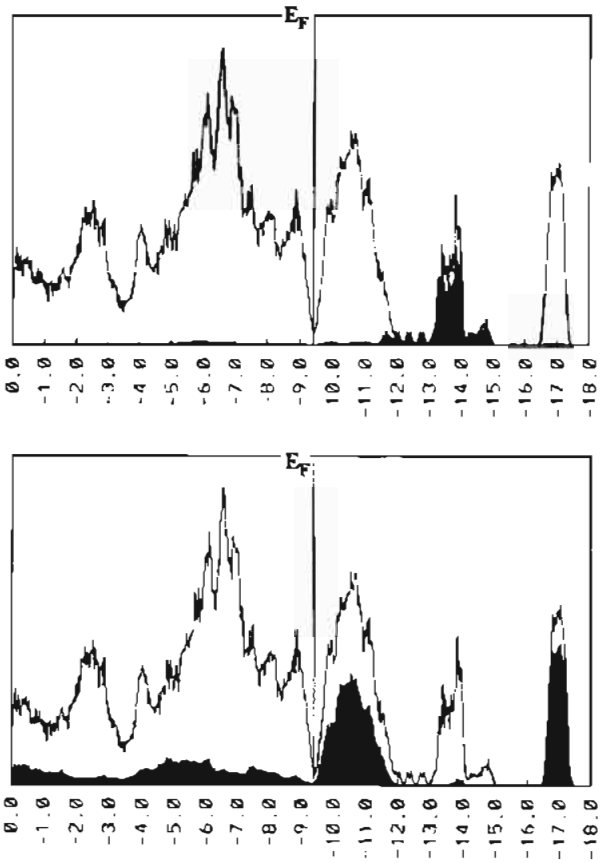

Figure 5. Total DOS for La_5Ge_3P with solid areas depicting atomic orbital projections of P (top) and Ge (bottom) states therein.

bonding components between Ge 4p and both metal atoms. The Fermi level E_F at −9.19 eV cuts across the lower portion of a largely La-based band. A notable feature of the band structure is the absence of a clear separation between the Ge p valence band and the metal-based conduction band. The large dispersion results from strong mixing of La with the Ge orbitals in the nominal valence band, as confirmed by inspection of the individual energy bands near the Fermi level in k space.

Both the orbital projections of the DOS and the La–Ge COOP (crystal orbital overlap population) curves, Figure 4, show that bonding of La with the Ge p_x and p_y orbitals normal to the chains (designated (xy)) are mainly responsible for this. A strongly antibonding interaction between intraplanar La2(xy) orbitals at about −11.5 (and −19) eV is combined with robust La2–Ge bonding in the lower part of the valence band. Surprisingly, the La1 atoms in the linear chains (Figure 1) are relatively weakly bonded (Figure 4; Table VI) despite the fairly short La1–La1 distances (Pauling bond order = 0.80); in other words, these bonding states are largely upopulated at this electron concentration, and the atoms' close proximity is apparently more of a matrix effect. Strong La–Ge interactions, as well as La–La interactions within the shared faces, dominate the bonding. Interestingly, the antibonding La2–La2 contributions within the valence bands are quite absent in the electron-richer and differently proportioned Zr_5Sb_3.[14] Substitution of a smaller rare-earth metal for lanthanum would possibly weaken these antibonding interactions as well. The La_5Ge_3 combination appears near the stability limit for Mn_5Si_3 types in terms of size proportions; La_5Si_3 and La_5As_3 evidently do not occur in this structure.[8]

The La–Ge COOP distribution shows that La–Ge bonding interactions are near a maximum at E_F, although some bonding La1–Ge interactions thereabove remain. In the framework of a rigid band approach, an electron count corresponding to a "La_5Pn_3" compound (E_F = 8.78 eV) would yield La–Pn interactions that are all bonding. Such electron-richer R_5Pn_3 phases in the

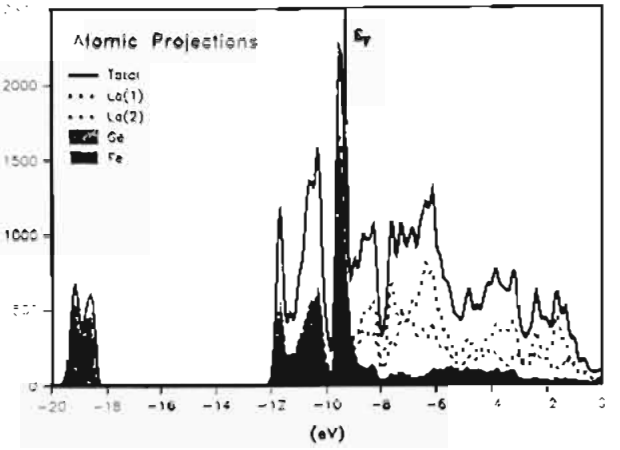

Figure 6. The DOS (solid) for La_5Ge_3Fe and atomic projections of La (dashed), Ge (shaded), and Fe (cross-hatched) contributions.

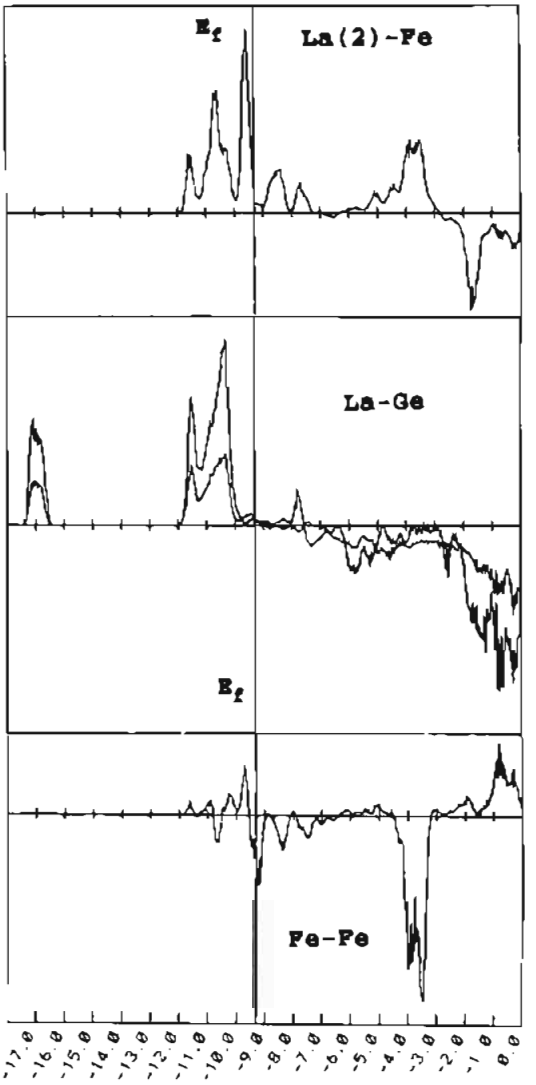

Figure 7. COOP curves for atom pairs in La_5Ge_3Fe: top, La2–Fe; middle, La2–Ge (upper) and La1–Ge; lower, Fe–Fe. The abscissa scales are arbitrary.

Mn_5Si_3-type structure are known for Sb and Bi and with substantially reduced c/a ratios (0.70–0.71[8]).

As expected, La_5Ge_3P is calculated to have an energy gap (~0.08 eV) at E_F between the Ge-derived valence band and the metal-based conduction band. This is illustrated by the compound's total DOS and the separate Ge and P atomic projections therein in Figure 5. A new P 3p (plus La2) band appears between about −15 and −12 eV. The Ge p and s bands mixed with La at

~−7.0 eV and around −10.5 eV, respectively, are much as before, while broad metal-derived conduction bands make up the structures above E_F. The La1–La1 interactions below E_F remain weak. Nearly optimal La–Ge bonding is achieved at the electron count of La_5Ge_3P, with some residual La–Ge bonding states above E_F, as before (Figure 4). The rise in E_F expected for La_5Ge_3S and La_5Ge_3Cl would not, in a rigid band approximation, add any major antibonding interactions except some between La2 atoms. The latter lie near E_F and particularly along the *c*-axis because of less involvement of these in La–Ge in-plane bonding, and their occupancy presumably contributes to the observed c/a increases. The marked La2–La2(z) population between those triangles is noticeably less in the La_5Ge_3P case, however. In terms of derived changes, the La2 is clearly oxidized on insertion of P, but not Fe (below). As also noted for Zr_5Sb_3S systems,[14] the A2–A2(z) bonding states and overlap populations are principally converted to A2–Z bonding in the encapsulation process.

An interesting question is the following: How and why does an energy gap, which is absent in the host La_5Ge_3, arise in La_5Ge_3P? We trace this to the interaction of phosphorus with the host bands where the large interactions developed between La2 and P lie more or less normal to the strong bridging La2–Ge effects. This perturbation leads to a bonding (stabilization) of the P bands and further antibonding destabilization of the La2 bands along *c* noted above. Thus the La2 bands, which make-up most of these near E_F in La_5Ge_3, effectively rise in energy with respect to the other host-derived bands, and an energy gap is formed. The small energy gap calculated, 0.08 eV, agrees fortuitously well with the observed electrical band gap (0.11 eV).

The less classical behavior of these systems with a more electropositive Z is demonstrated in La_5Ge_3Fe, for which the DOS of the band structure are shown in Figure 6. The two La–Ge valence bands remain much as before. The bands from Fe d together with the lanthanum-derived bands form a broad structure that ranges from ~−10 eV to above E_F, while E_F cuts across the Fe d band at a high density of states. The DOS atomic orbital projections also show some overlap between the s (~−9.5 to −8.0 eV) and d bands (~−10.0 to −9.0 eV) of Fe.

The orbital interactions in La_5Ge_3Fe can be better appreciated with the COOP plots in Figure 7. The La–Ge bonding states of the host are nearly filled and maximized at E_F. These should not be significantly perturbed by smaller or larger electron counts in neighboring Z, which involve instead mainly iron-like d and s states. The COOP curve for La–Fe interactions reveals strong bonding from mixing of Fe s, d states with the La d orbitals. However, these interactions in the La_6Fe cluster unit do not result in significant "splitting" of the iron d bands, probably because of the contracted nature of Fe d orbitals. Thus, the electrons residing in these orbitals are practically localized, while the delocalized members lie in a broadened Fe s band that extends below E_F. Weak La1–La1 interactions are also deduced by the COOP curves. Overlap between the germanium- and lanthanum-based bands found in La_5Ge_3 is removed by iron interactions with La2, as in La_5Ge_3P, but the Z-induced gap between these is now filled by iron d-states. Bonding trends associated with the Co, Ni, Cu, Zn progression would be interesting to explore.

These results also contribute significantly to possible interpretations of the magnetic characteristics of the soft ferromagnetic La_5Ge_3Fe as well as XPS core shifts of this and other derivatives. These will be integrated into an article on $La_{15}Ge_9Z$ phases and reported at a later time.[33]

Acknowledgment. L. Wolfe and S. Sevov assisted measurably in the four-probe and Q resistivity measurements, respectively, J. Ostensen provided the magnetic data, and G. J. Miller and M. Kertesz contributed to the calculational efforts.

Supplementary Material Available: Tables of data collection and refinement details and anisotropic displacement parameters for La_5Ge_3 and La_5Ge_3Cr (2 pages). Ordering information is given on any current masthead page.